LA-UR-18-31380
Approved for public release; distribution is unlimited.

Title: Review of PBX 9502 Pop Plot data

Author(s): Menikoff, Ralph

Intended for: Report

Issued: 2018-12-06

Review of PBX 9502 Pop Plot data

Ralph Menikoff

December 3, 2018

Abstract

Pop plot data (distance of run and time to detonation as a function of shock pressure) is a simple characterization of shock initiation of a high explosive. It is used, along with other data, to calibrate reactive burn models. For the insensitive TATB based explosive PBX 9502, there are data at 5 initial temperatures (77 K, -55 C, 23 C, 76 C, 130 C) and for several lots. Here we review the dependence of the Pop plot on temperature and the variation with lot. There is a significant increase in shock sensitivity with temperature. Since the Pop plot is important for modeling, fit parameters are interpolated to cover the temperature range $-55 < T < 76$ C. The scatter in the data and variation with lot is important for assessing the accuracy to which a model can be calibrated.

1 Introduction

For a high explosive (HE), a key characterization of a shock-to-detonation transition (SDT) driven by a planar shock is the distance-of-run and time to detonation. Both the run distance (x) and run time (t) as a function of shock pressure (P) on a log-log plot are well approximated by a straight line. This relation was first observed by Ramsay and Popolato [1965], and is know as a Pop plot. For reactive burn models, Pop plot data are used to calibrate the burn rate below the CJ pressure, which is the pressure regime that dominates shock initiation.

The Pop plot is also used to gauge the relative shock sensitivity of HEs. If the Pop plot shifts up in the (P, x)-plane then for a given shock pressure, the run distance to detonation is larger and the explosive is less sensitive. Similarly, if the Pop plot shifts down, the run distance is smaller and the explosive is more sensitive. For a given HE, experiments have shown (see for example [Campbell et al., 1961] and [Gibbs and Popolato, 1980, part II, § 4.1]) that the sensitivity increases when either the initial temperature or the porosity of the reactants increases. This is the expected behavior based on the ignition and growth concept of hot spots; see for example [Lee and Tarver, 1980] or [Menikoff and Shaw, 2010].

Decreased shock sensitivity at low temperature or at low porosity can be an issue for reliably detonating an HE. At the other extreme, increased shock sensitivity at high temperature or as the density decreases (higher porosity) can be an issue for accident scenarios. Thus, the temperature dependence of the Pop plot is important for a modeling HE response.

Plastic-bonded explosives are an important class of HEs. They are heterogeneous materials composed of explosive grains, polymeric binder and a couple of percent of porosity. The PBXs are manufactured in lots. The statistics of the heterogeneities can vary with lot, and affect the distribution of hot spots generated by a shock wave. This would affect the burn rate, and hence the Pop plot. Variations of the Pop plot with lot have been observed experimentally, and can limit the accuracy to which a burn rate can be calibrated.

In this report we review the Pop plot data for the TATB based PBX 9502. This is an insensitive HE for which there is a large amount of data. The Pop plot data discussed here are at 5 temperatures and for several lots (both virgin and recycled dry animated TATB). The range of temperatures is beyond the standard operating range of -55 to 75 C.

The data is taken from the following published sources:

1. very cold, -196 C (77 K); [Hollowell et al., 2014]
2. cold, -55 C (218 K); [Gustavsen et al., 2012, 2005]
3. ambient, 23 C (296 K); [Dick et al., 1988, Gustavsen et al., 2006]

4. hot, 76 C (349 K); [Dallman and Wackerle, 1993, Gustavsen et al., 2017]

5. very hot, 130 C (403 K); [Gustavsen et al., 2018]

There is also Pop plot data at very high temperature, 252 C (525 K). This data is not used here since experiments have shown that the PBX mass decreases by about 1 percent in the 'soak' time needed to achieve a uniform temperature; see [Dallman and Wackerle, 1993, fig. 1] and [Maienschein and Garcia, 2002, fig. 6]. The loss of mass potentially adds porosity and depending on what outgasses can slightly change the chemical composition.

In section 2 we discuss shock-to-detonation transition experiments used to obtain a point on the Pop plot and fitting Pop plot data from a series of experiments. The variation of the PBX 9502 Pop plot with both temperature and lot are discussed in section 3. We show in section 4 that the Pop plot parameters can be interpolated to obtain the Pop plot for all temperatures over the standard operating range. The last section is a summary of the Pop plot fits to the SDT data, and briefly discuss other types of shock initiation experiments.

2 Background

Two types of experiments have been used to obtain a point on the Pop plot. The older type, called wedge experiments, are described in Gibbs and Popolato [1980, see §4.1]. A shock is driven into a wedge shaped HE sample by an explosive drive system consisting of plane wave lens, booster HE and an inert attenuator. The booster and attenuator are used to vary the initial shock strength and to minimize the pressure gradient behind the shock driving the HE. A streak camera is used to measure the $x(t)$ trajectory as the lead shock breaks out on the downstream surface of the wedge. With a wedge angle of 30 to 40 degrees, the shock break out runs ahead of side rarefactions. Consequently, the measured trajectory corresponds to that of a planar reactive wave. The experiment also measures the shock or particle velocity in the attenuator prior to impacting the HE sample. The initial shock pressure is determined from the impedance match utilizing the equation of state (EOS) of the attenuator, and the initial slope of the shock trajectory from the streak record.

The newer type of experiments use a projectile from a gas gun to drive a planar shock into a cylindrical sample of HE. A thin magnetic gauge package [Gustavsen et al., 2006, fig. 1] is embedded in the HE sample at an angle similar that used for the wedge experiments. The gauge package has both tracker gauges and velocity gauges. The tracker gauges measure the lead shock trajectory. The initial HE shock pressure is determined by the impedance match of the projectile

impacting the HE. The velocity gauges measure Lagrangian time histories of the particle velocity. Thus, these experiments provide more information than the wedge experiments.

The shock trajectory for both types of experiment is effectively discretized in space every 1 to 2 tenths of mm, which corresponds to time intervals of about 40 to 20 ns for shock velocities of 4.5 to 8 km/s. The trajectory is smoothed to calculate the first and second derivatives, *i.e.*, shock velocity and acceleration, respectively. The transition to detonation is taken as the point for which $u_s(t)$ is steepest; *i.e.*, the maximum acceleration. An estimate for the error in the transition point is roughly twice the discretization interval; ± 0.3 mm in x and ± 50 ns in t.

For the gas gun experiments, the transition can also be based on the amplitude and shape of the time histories from the velocity gauges. The spacing of the gauges (about 0.5 mm) gives an estimate of the uncertainty of the transition point.

Pop plot data is typically in the range of run distances from about 1 to 40 mm. Longer run distances (lower shock pressures) are limited by the width of the HE and side rarefaction which cause the 1-D interpretation of the shock trajectory to break down. We also note that the straight line Pop plot fit breaks down at low pressure. This has been observed for HMX based explosive by Vandersall et al. [2010]. It is also expected from the perspective of hot spots as elastic-plastic or visco-elastic effects smear out the shock profile for low shock pressures and make pore collapse a less effective means of generating hot spots. The smearing and low burn rate has been observe for HMX crystals and PBX 9501 by Dick et al. [1998, 2004].

Shorter run distances (high shock pressure) have fewer trajectory points up to detonation which lead to a large relative error for the transition point. In addition, a high initial shock pressure results in a large reaction rate that makes it difficult to determine the initial shock pressure. Typically, Pop plot data is below the CJ pressure and for run distances greater than the steady state reaction-zone width. For PBX 9502, the ambient CJ pressure is 28 GPa. TATB has a fast and slow reaction rate. The fast rate dominates the detonation transition. The fast reaction time and reaction width are estimated to be about 15 ns and 0.2 mm, respectively.

The next section shows that the data has a scatter which is partly random and partly systematic. The largest random uncertainties are likely to be from the measurement of the initial shock pressure and the sample-to-sample variation of the initial density and initial temperature. We estimate the uncertainty in the initial pressure to be $\pm 2\,\%$, due to the uncertainty in the initial particle velocity that enters the shock jump condition for the pressure $P = \rho_0\, u_p u_s$.

The reported sample-to-sample variation is ± 2 K in temperature and on the order of ± 2 mg/cc in density within a lot plus 2 to 4 mg/cc among lots out of 1.890 g/cc. Based on the temperature interpolation of the Pop plot in section 4, the initial temperature uncertainty results in a 1.5 percent change in the run distance. Though the variation in initial density is small (about $0.1\,\%$), we note that the change in porosity is much larger (a few percent). Porosity affects

the burn rate and hence the transition point. It is clear that shock sensitivity increases with porosity (lower density). But due to limited data available at other initial densities, it is difficult to quantify the effect on the transition point of a a small variation in the initial density of PBX 9502. However, for LX-17 which is a TATB based explosive very similar to PBX 9502, a density difference of 13 mg/cc out of 1.900 g/cc makes a significant difference on the Pop plot; see [Gustavsen et al., 2002, fig 4].

Experimental uncertainties also arise from slight misalignments of the sample HE with the drive system. Here we note the effect of tilt, that is, the angle between the gas gun projectile and the surface of the HE sample. Similar considerations apply to the explosive drive system for the wedge experiments.

Depending on the tilt orientation, either the rise time of the lead shock for the velocity gauges and the time offset between top and bottom tracker gauges, or the angle of the shock front relative to the surface of the HE are affected. Typically, the tilt angle is about 10 milliradians. The effect on the shock rise time and offset between the tracker gauges can be as much as 50 ns. This would affect the uncertainty of a point on the shock trajectory. The angle of the shock front can change the apparent shock speed at the gauges by up to 4.5 % [Gustavsen et al., 2012, §III.B]. This would add to the relative error of the shock trajectory.

The leading systematic difference is with the initial temperature. Experiments with different lots were aimed at checking for HE grain size effects on shock initiation that have been observed for other PBXs; see discussions in [Gustavsen et al., 2006, §V.A] and [Gustavsen et al., 2012, §IV.B]. The PBX 9502 experiments show a significant difference with some lots at cold temperature but not at ambient temperature.

2.1 Linear fit to Pop plot data

The Pop plot is a linear fit to the data on a log-log scale; *i.e.*,

$$\log(x/\text{mm}) = A_x - B_x \log(P/\text{GPa}) \ , \tag{1a}$$

$$\log(t/\mu\text{s}) = A_t - B_t \log(P/\text{GPa}) \ . \tag{1b}$$

For run distance to detonation, the coefficients A_x and B_x are chosen to minimize the residual

$$\text{residual} = \sum_i [\log(x_i) - \log(x_{fit}(P_i))]^2 \ . \tag{2}$$

To leading order in $x - x_{fit}(P)$,

$$\begin{aligned}\log(x) - \log(x_{fit}) &= \ln(x/x_{fit})/\ln(10) \\ &= \ln[1 + (x - x_{fit})/x_{fit}]/\ln(10) \\ &\approx \big[(x - x_{fit})/x_{fit}\big]/\ln(10) \ .\end{aligned}$$

Consequently, to leading order the linear fit corresponds to minimizing the root mean square relative error,

$$\text{rms rel error} = \left(N^{-1} \sum_{i=1}^{N} \Big[\big(x_i - x_{fit}(P_i)\big)/x_{fit}(P_i) \Big]^2 \right)^{1/2} \ , \tag{3}$$

and similarly for the time to detonation with x replaced by t. For all the Pop plot fits to the data in the next section, the rms rel error is given as a measure of the scatter in the data points.

A linear fit typically assumes that the independent variable is exact and all the uncertainty is in the dependent variable. For the Pop plot data there is an uncertainty in both variables. The uncertainty in P can be shifted to an uncertainty in the relative error, $\Delta x/x = B\,\Delta P/P$ and similarly for t. With $B \approx 3$ a $\pm 2\,\%$ error in P implies about a $\pm 6\,\%$ relative error in x or t. Similarly, small misalignments in an experiment, such as tilt discussed in previous subsection, would contribute a few percent to the relative errors. If the measurement uncertainties are random, then the fit should be more accurate than the values of the data points.

A linear relation on a log-log plot implies a power law behavior

$$x/\text{mm} = 10^{A_x} \cdot (P/\text{GPa})^{-B_x} \ , \tag{4a}$$

$$t/\mu\text{s} = 10^{A_t} \cdot (P/\text{GPa})^{-B_t} \ . \tag{4b}$$

Furthermore, the run distance and the time to detonation are related by a power law

$$x/\text{mm} = 10^{A_x - A_t B_x/B_t} \cdot (t/\mu\text{s})^{B_x/B_t} \ . \tag{5}$$

We note that the power B is independent of units while A does depend on the choice of units for P and either x or t.

3 Pop plot data

The complete Pop plot data set consists of 99 experiments with 1 data point per experiment. The data are shown in fig. 1 for all temperatures and all lots. Pop plot parameters are fit separately for each temperature. They are listed in table 1. Outliers are excluded from the parameter fits. The outliers are discussed in the following subsections.

Table 1: Pop plot parameters fit to data at each temperature.

T (C)	lots	A_x	B_x	rel err (%)	A_t	B_t	rel err (%)	shots	B_x/B_t
-196	1	4.985	3.364	3.5	4.564	3.682	4.5	5	0.914
-55	5	4.607	3.211	5.5	4.247	3.563	5.1	33	0.901
23	5	4.113	2.920	7.4	3.706	3.226	7.9	37	0.905
76	2	3.442	2.516	5.0	3.049	2.816	4.6	21	0.893
130	1	2.828	2.200	1.5	2.461	2.529	2.9	3	0.870

Several general trends are seen in the fig. 1 and table 1:

1. Shock sensitivity increases with initial temperature.
2. There is a scatter in the data for each temperature. The relative errors for run distance and time to detonation are comparable.
3. At cold temperature, there is a systematic variation with lot that exceeds the scatter in the data. This will become more apparent in the 'cold data' subsection below. At the very cold temperature, there is data for only 1 lot. So it is not known whether or not lot dependence persists at colder temperatures.
4. The slope of the Pop plot decreases as the initial temperature increases.
5. The exponent for $x(t)$ in Eq. (5) is less than 1 and tends to decrease with temperature.

The rms relative error in the fits is largest for the ambient case at 7.4 and 7.9 % for run distance and run time, respectively. This is comparable to the estimated error in the previous section. Including the outliers would significantly increase the relative error to 11.2 and 10.8 % for run distance and run time, respectively. With respect to Pop plot parameters in table 1, the relative error of the outliers can be as high as 30 %. We note the data for the ambient case covers the widest range in pressure; from 7.5 GPa to 25 GPa, which is slightly below the CJ pressure. Larger ranges are more constraining on the slope of the Pop plot.

An interesting point is that the porosity of PBX 9502 decreases with temperature; see [Dallman and Wackerle, 1993, fig 3]. This is based on the values of the coefficient of thermal expansion for 9502 and its components. Data for other PBXs shows that shock sensitivity increases with porosity; see for example [Gibbs and Popolato, 1980, part II, § 4.1]. Thus the change in porosity with temperature tends to offset the increase in sensitivity with temperature. This implies distinct effects on the hot-spot distribution from porosity and temperature.

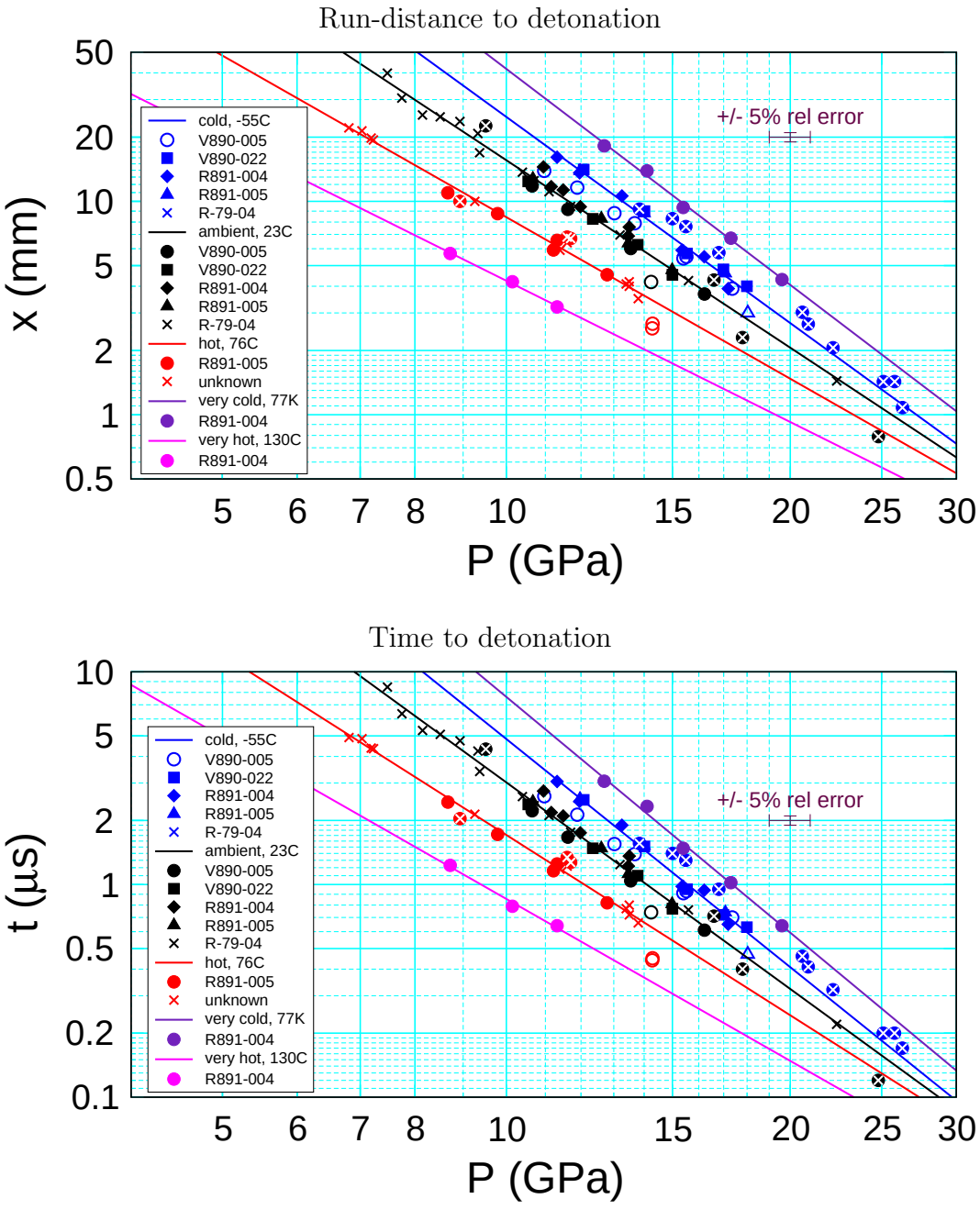

Figure 1: Pop plot data for PBX 9502. Symbols are for gas gun experiments and 'x' for wedge experiments. Open symbols are outliers excluded from linear fit. Lines are fit to data at each temperature. As a guide, ±5% error bar is shown.

However, more recent neutron scattering experiments show that the porosity of PBX 9502 increases with temperature [Armstrong and Mang, 2018, fig 6]. Also, based on component thermal expansion, for TATB based LX-17, there is a temperature interval with increasing porosity. Moreover, thermal cycling of PBX 9502 leads to a change in density and hence porosity [Gustavsen et al., 2010]. It has been suggested that porosity can be affected by internal stresses at grain contacts which are partially relieved when temperature is varied. Consequently, the Pop plot may be affected by more than just the initial temperature and lot.

3.1 Ambient data

Most HE experiments are done at ambient temperatures, and consequently there are more ambient Pop plot data points than at any other temperature. The ambient Pop plot data for 5 lots are shown in fig. 2. Pop plot parameters fit separately to each lot are listed in table 2.

The fits were first done with all the data points. A point with a residual twice the root mean square was considered an outlier. The fit was redone excluding the outliers. After 2 iterations no further outliers occurred. There is 1 outlier out of 5 data points for lot V890-005 and 4 outliers out of 18 data points for lot R-79-04. The relative error of the outliers is in the range of 20 to 30 %. We also note that the data point relative errors for run distance and for time to detonation have the same sign. The correlation implies that the uncertainties in x and t are causally related.

The rms relative error for the lots varies from 1 to 7 %. However, the number of data points per lot (from 4 to 14 excluding outliers) is insufficient to get good statistics on the uncertainties. The largest number of data points is for the wedge experiments on lot R-79-04. This data set

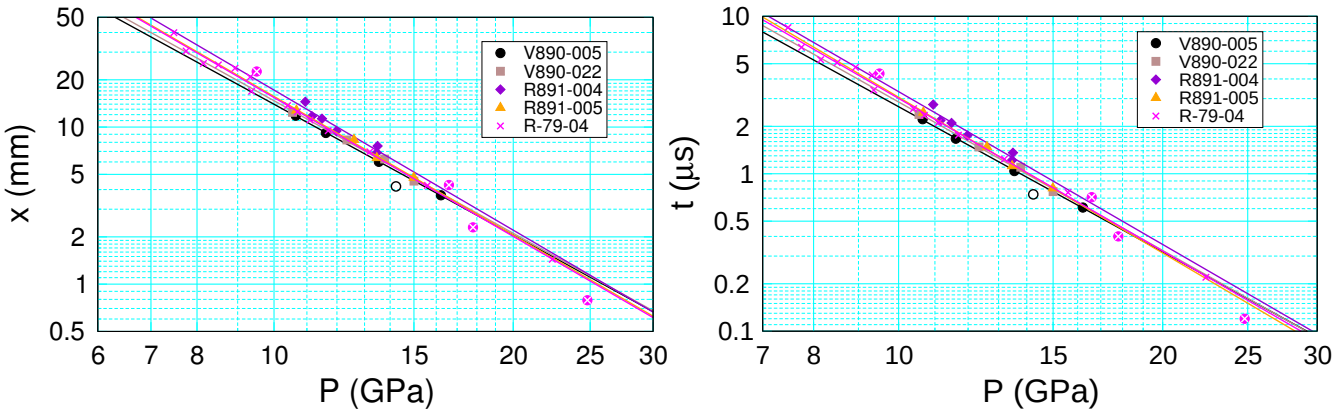

Figure 2: Pop plot data for ambient PBX 9502. Symbols are for gas gun experiments and 'x' for wedge experiments. Open symbols are outliers excluded from linear fit. Lines are fits to each lot.

Table 2: Pop plot parameters for each lot at ambient temperature.

lot	A_x	B_x	rel err (%)	A_t	B_t	rel err (%)	points	outliers
V890-005	3.912	2.766	0.5	3.490	3.064	0.9	4	1
V890-022	3.971	2.803	3.3	3.589	3.133	3.3	4	0
R891-004	4.198	2.963	6.3	3.746	3.225	6.7	6	0
R891-005	4.127	2.932	2.8	3.772	3.287	2.3	4	0
R-79-04	4.124	2.936	6.3	3.701	3.223	6.7	14	4
all	4.113	2.920	7.4	3.706	3.226	7.9	32	5

has the largest relative error. It also has the largest pressure range, 7.5 to 25 GPa. If only the data points within the pressure range of the gas gun experiment, 10 to 17 GPa, are used then the rms relative error of the Pop plot fit drops to 1.2 %, which is one of the lowest for all the lots. Overall the slopes for all data sets are about the same, and in the pressure range of the gas gun experiments there is systematic shift in x or t between lots of 10 to 20 %. Considering the difference in lots and the scatter in the data, there does not appear to be a significant difference between the Pop plot data obtained from the wedge experiments and gas gun experiments.

Also shown in table 2 are parameters for fit to the combined data of all the lots. These parameters are used in fig. 1 and table 1. The rms relative error is larger for the combined data sets then for any of the lots. This is due to the systematic shift in x or t among the lots.

Figure 3 shows an example of run distance versus time to detonation based on the Pop plot fits for run distance and time to detonation, Eq. (5). Since the exponent is slightly less than 1 ($x \propto t^n$), the curve is slightly concave.

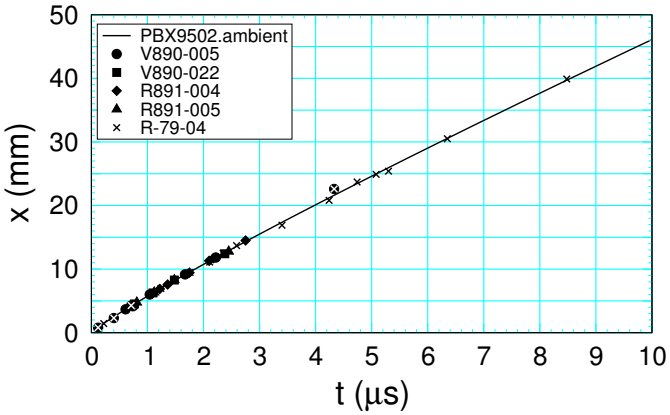

Figure 3: Run distance versus time to detonation from ambient PBX 9502 based on Pop plot fits.

3.1.1 Outlier

The Pop plot for lot V890-005, based on gas gun experiments [Gustavsen et al., 2006, fig 2], had 1 outlier (with relative error of 20 %) as seen in fig. 4. Next we examine the data for the outlier (shot 2s43 at $P_s = 14.24$ GPa) and the neighboring data point (shot 2s86 at $P_s = 13.55$ GPa). The tracker and gauge data are taken from the LANL small scale database.

The velocity and tracker gauge data are shown in fig. 5 along with the transition point from [Gustavsen et al., 2006, fig 2]. Based on the transition time and the shock jump off time, for shot 2s43 the transition is near the velocity gauge at 4.29 mm, while for 2s86 the transition is near gauge at 5.85 mm. Comparing these gauges, the transition profile is less sharp and the peak velocity lower for shot 2s43 than for 2s86. Thus, the stated transition point would appear to be relatively early for 2s43 compared to 2s86. Another difference between the shots is that the peak velocity after transition increases for 2s86 whereas it is almost constant for 2s43.

The tracker gauges show that the detonation speed (lead shock velocity just above the transition) is low for 2s43 (7.14 km/s) compared to 2s86 (7.73 km/s). Based on extrapolating diameter effect data of Campbell [1984], the CJ detonation speed is 7.78 km/s. Related to the difference in detonation speed, the zoomed tracker gauge plot shows the transition is more abrupt for shot 2s43 than for 2s86; *i.e.*, distance between guide lines for the initial shock speed and detonation speed, and the trajectory data points is smaller for 2s43. The qualitative differences in the behavior around the transition may be due to inaccuracies in the data or sample-to-sample differences in the grain scale heterogeneities of the HE, which would affect the burn rate.

We note that there is a time shift (10 to 12 ns) between the top and bottom tracker gauges of 2s86. This is likely due to tilt between the gas gun projectile and the HE sample. For shot 2s43, there is data for only 1 tracker gauge, so there is no information to infer tilt.

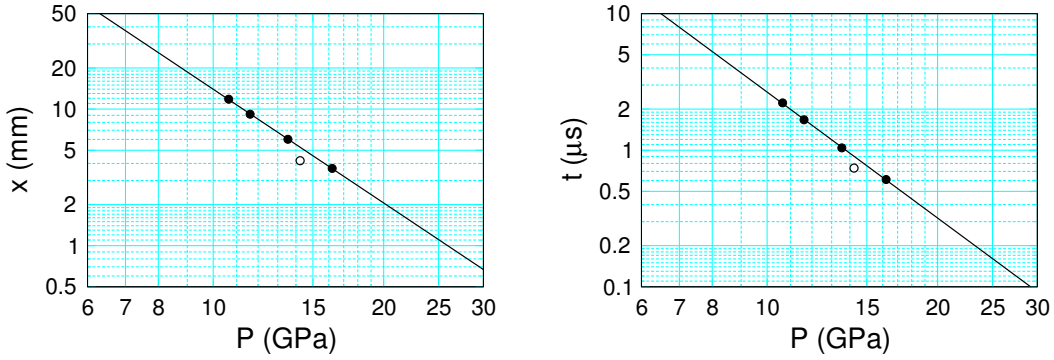

Figure 4: Pop plot data points for PBX 9502 lot V890-005 at ambient temperature. Outlier corresponds to gas gun shot 2s43 with shock pressure of 14.2 GPa.

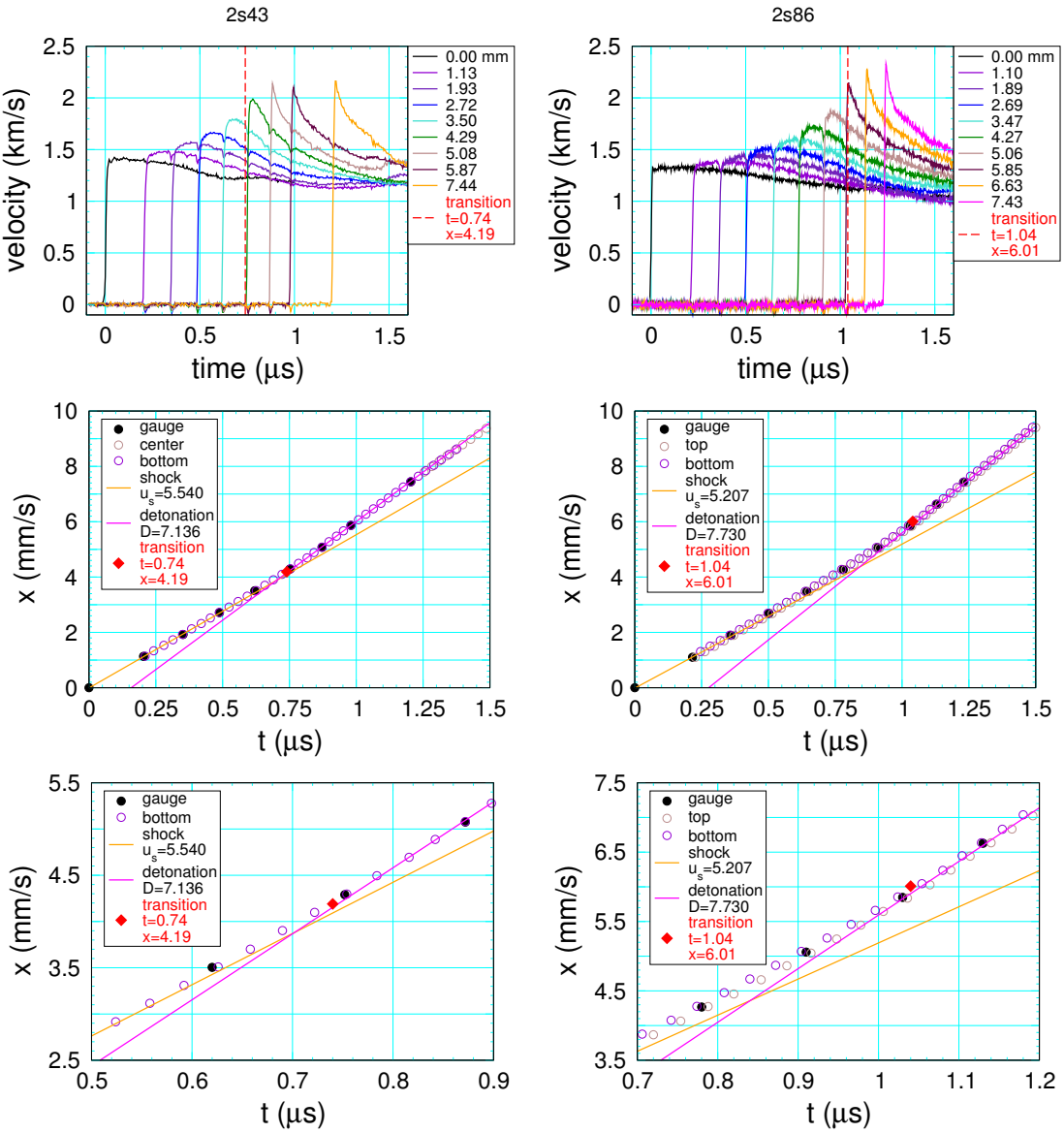

Figure 5: Gauge data for shots 2s43 and 2s86. Top plots are Lagrangian velocity profiles at initial positions listed in the legend; $x = 0$ corresponds to projectile/9502 interface. Transition time from [Gustavsen et al., 2006, fig 2] indicated by vertical dashed red line. Middle plots are tracker data and shock jump off time from the velocity gauges. The orange and magenta lines correspond to fits of the first 10 data point and 10 data points after transition to detonation, respectively. The bottom plot zooms in on the tracker data about the transition point. Transition point from [Gustavsen et al., 2006, fig 2] is denoted by red diamond.

The lead shock speed can be obtained from the tracker gauge data. Typically, the tracker data is smoothed by fitting to a function and then taking the analytic derivative of the smoothing function to obtain the shock speed, $u_s = \mathsf{d}x/\mathsf{d}t$. The transition point can be taken to correspond to the point at which the shock speed changes most rapidly; *i.e.*, the point of maximum acceleration. This leads to an automated procedure that determines an objective transition point. In principle, if there are sufficient points in the transition region and the fitting form represents the transition region well, then the approach with the fitting function should reduce the scatter in Pop plot data points, which would enable more accurate coefficients for the Pop plot fit.

Nevertheless, it is instructive to examine the shock speed obtained from a simple finite difference approximation of the time derivative $u_s\left(\frac{t_1+t_2}{2}\right) = \frac{x(t_2)-x(t_1)}{t_2-t_1}$, as shown in fig. 6. The velocity is noisy due to round off errors and the limited precision of the data. Even with the noisy data, one can obtain rough bounds on the transition point based on where the shock speed changes most rapidly: $4 < x < 5.5\,\text{mm}$ for shot 2s43 and $5 < x < 6.5\,\text{mm}$ for shot 2s86. We note that there are only about 6 data points within the bounds. The indicated transition point for 2s86 is closer to the detonation speed end of the interval while for 2s43 is closer to the shock speed end. Since the burn rate increase with shock strength, the transition should be closer to the detonation speed end of the interval.

It would be reasonable to regard the transition for 2s43 to occur later than the value selected by [Gustavsen et al., 2006, fig 2]. In particular, transition point at the following gauge with x=5.08 mm and shock jump off time of $t = 0.87\,\mu\text{s}$ in fig. 5. This would be much closer to the Pop plot fit shown in fig. 4, which at the outlier shock pressure is $x = 5.26\,\text{mm}$ and $t = 0.90\,\mu\text{s}$, and give relative errors for x and t of 3.4 % and 3.3 %, respectively.

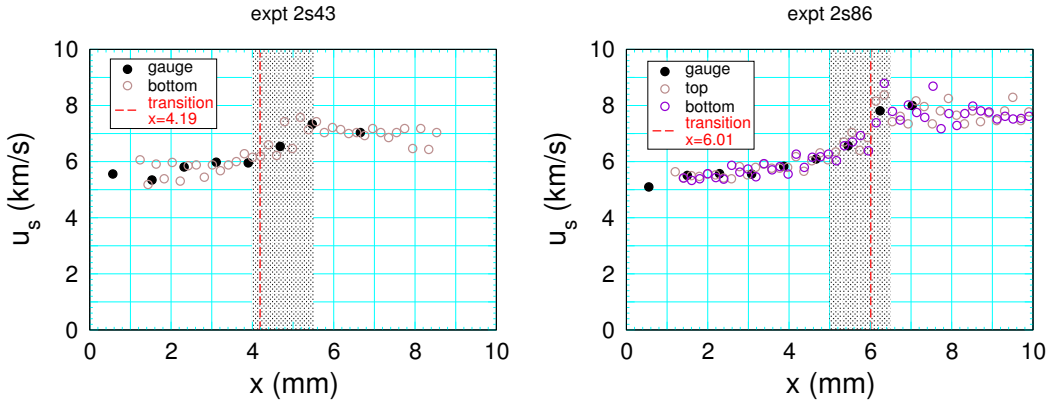

Figure 6: Shock speed for shots 2s43 and 2s86 from finite differences of tracker gauge data. Transition run distance from [Gustavsen et al., 2006, fig 2] is indicated by the vertical dashed red line. Shaded region indicates interval in which shock speed changes rapidly.

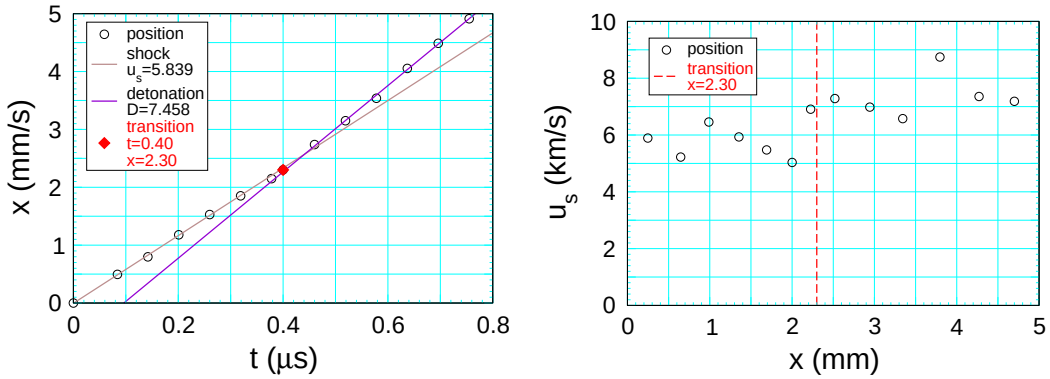

Figure 7: Trajectory and finite difference shock velocity for shot E4738. Transition point from [Dick et al., 1988, table 1] is indicated by red diamond and vertical dashed red line.

For the wedge experiments, lot R-79-04, there are 4 outliers seen in fig. 2. The trajectory data is only available for 1 outlier, shot E4738 at $P_s = 17.8\,\mathrm{GPa}$. The trajectory and shock velocity are shown in fig. 7. The transition point can be selected as the next data point at $x = 2.70\,\mathrm{mm}$ and $t = 0.46\,\mu\mathrm{s}$. This would give relative errors for x and t of 4.9 % and 2.1 %, respectively. Thus, the choice of the transition point can explain the discrepancy in the outliers.

3.2 Cold data

There are almost as many Pop plot data points at cold temperature as there are at ambient temperature. The data for 5 lots are shown in fig. 8. Pop plot parameters fit separately to each lot are listed in table 3. We note that there are no cold data points below 11 GPa, whereas the

Table 3: Pop plot parameters for each lot at cold temperature.

lot	A_x	B_x	rel err (%)	A_t	B_t	rel err (%)	points	outliers
V890-005	4.064	2.797	1.9	3.497	2.959	2.9	7	0
V890-022	4.612	3.204	4.5	4.250	3.563	3.9	5	0
R891-004	4.697	3.299	5.7	4.271	3.586	6.4	6	0
R891-005	4.605	3.210	4.2	4.239	3.556	4.1	4	1
R-79-04	4.835	3.342	5.6	4.374	3.360	6.5	10	0
all	4.299	2.952	11.1	3.867	3.239	10.8	32	1
middle 3	4.607	3.211	5.5	4.247	3.563	5.1	15	1

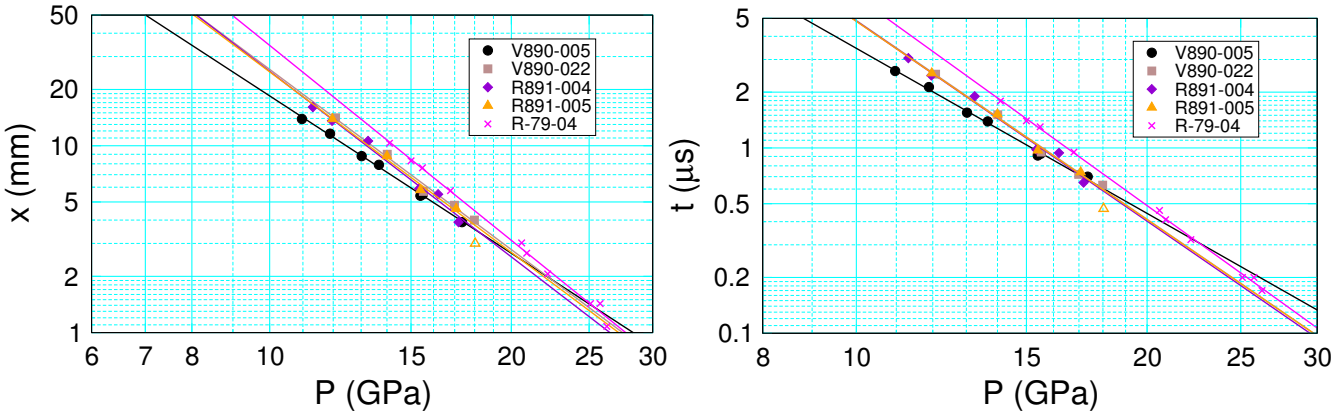

Figure 8: Pop plot data for cold PBX 9502. Symbols are for gas gun experiments and 'x' for wedge experiments. Open symbols are outliers excluded from linear fit. Lines are fits to each lot.

ambient data for lot R-79-04 extends down to 7.5 GPa. The largest run distance for the cold Pop plot data is 16 mm. Thus, experiments could be done at lower pressure.

The rms relative errors for the cold lots (2 to 6.5 %) are comparable to those for the ambient lots. However, the Pop plot fits are qualitative different in that the slopes have a large variation such that the Pop plot lines cross within the range of the data. That is to say, the systematic differences among lots are quite significant.

The Pop plot for lots V890-022, R891-004 and R891-005 are very similar. Table 3 also gives fits to the combined data for the above 3 lots, and for the combined data of all 5 lots. Due to systematic differences for the lots, the rms error for the fit to all the data is much larger than that of the individual lots. The rms relative error for the 3 lots combined is similar to that of the lots separately. The trade-off is that the data points for the other 2 lots (V890-005 and R-79-04) have large relative errors.

We note that including more data sets improves the accuracy of a fit if the uncertainties are random but not if the data sets have different systematic errors. For fig. 1 and table 1 we have chosen to use the parameters for the 3 combined lots.

3.2.1 Outlier

The Pop plot for lot R891-005, based on gas gun experiments [Gustavsen et al., 2012], had 1 outlier (shot 2s302 at $P_s = 18.03\,\mathrm{GPa}$ with relative error of 20 %) as seen in fig. 9. Next we examine the gauge data taken from the LANL small scale database.

The velocity and tracker gauge data are shown in fig. 10. There is a time offset between the top and bottom trackers that indicates projectile was tilted relative to the PBX 9502 sample. Both the velocity time histories and the shock velocity indicate that the stated transition point ($0.47\,\mu\mathrm{s}$ and 3.0 mm) is early. A better choice for the transition point would correspond to the next velocity gauge at 3.41 mm with jump off time of $0.534\,\mu\mathrm{s}$. This would reduce the relative error of the fit for t and x roughly in half, to 9.4 % and 9.1 %, respectively.

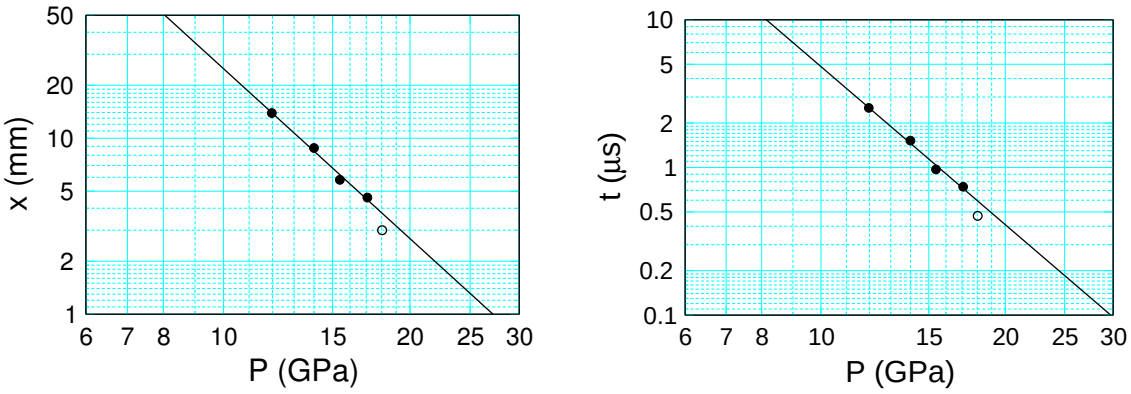

Figure 9: Pop plot data points for PBX 9502 lot R891-005 at cold temperature. Outlier corresponds to gas gun shot 2s302 with shock pressure of 18.0 GPa.

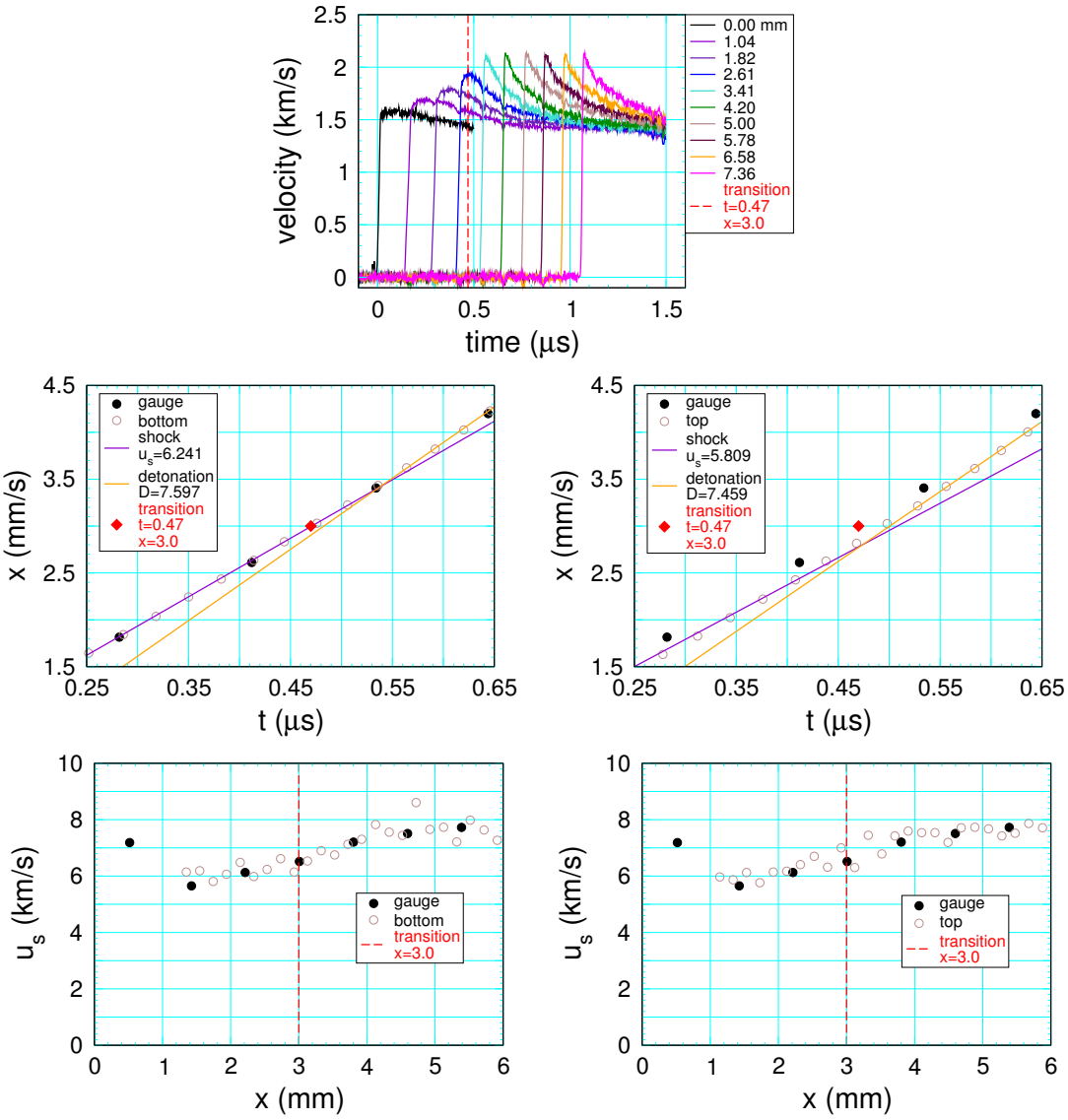

Figure 10: Gauge data for shot 2s302. Top plot is velocity gauge data. Vertical dashed red line is transition time from [Gustavsen et al., 2012, 2005, fig 10]. Middle plots are tracker data for bottom and top tracker, respectively. Also shown are the shock jump off time from the velocity gauges. The orange and magenta lines correspond to fits of the first 10 data point and 10 data points after transition to detonation, respectively. Transition point from [Gustavsen et al., 2012, 2005, fig 10] is denoted by red diamond. Bottom plots are finite difference shock velocity from the tracker gauges.

3.3 Hot data

At the hot temperature there is data for only 2 lots. The data are shown in fig. 11, and the parameter fits are listed in table 4. The rms relative error, with outliers excluded, are comparable to the ambient case.

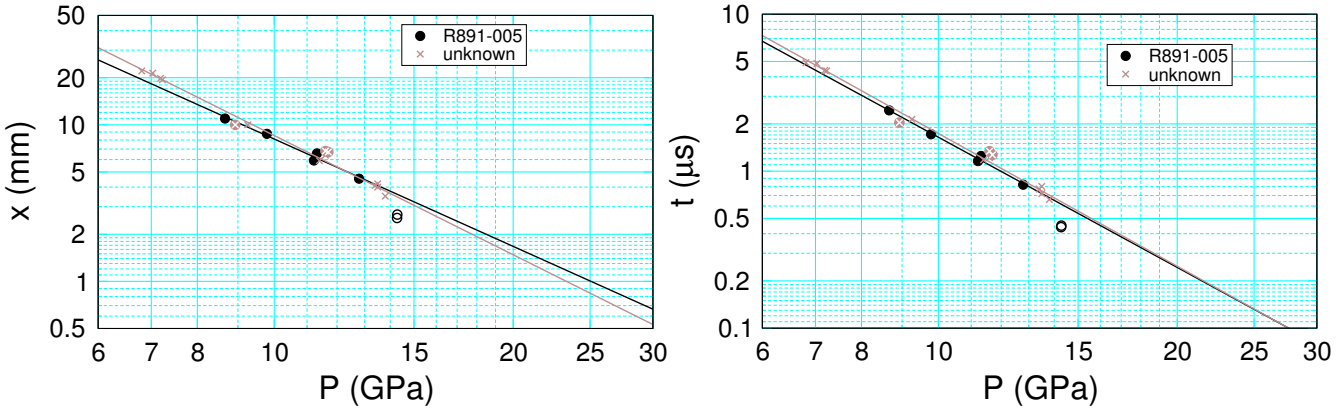

Figure 11: Pop plot data for hot PBX 9502. Symbols are for gas gun experiments and 'x' for wedge experiments. Open symbols are outliers excluded from linear fit. Lines are fits to each lot.

Table 4: Pop plot parameters for each lot at hot temperature.

lot	A_x	B_x	rel err (%)	A_t	B_t	rel err (%)	points	outliers
R891-005	3.188	2.278	4.5	2.971	2.755	3.6	5	2
unknown	3.462	2.531	4.3	3.050	2.810	4.0	11	3
all	3.442	2.516	5.0	3.049	2.816	4.6	16	5

3.3.1 Outlier

The Pop plot for lot R891-005 has 2 outlier as seen in fig. 11; shots 2s390 and 2s418 with relative errors of 25 to 30 %, respectively. Figure 12 shows the gauge data for the outliers. The tracker plots indicate that the transition to a detonation is very abrupt. Based on the shock velocity plot we estimate the transition to occur at about 3 and 3.1 mm for 2s390 and 2s418, respectively. This would reduce the relative error in half, less than 15 %. For 2s418 there is a second tracker gauge which gives different detonation speed after the transion. Part of the large relative error

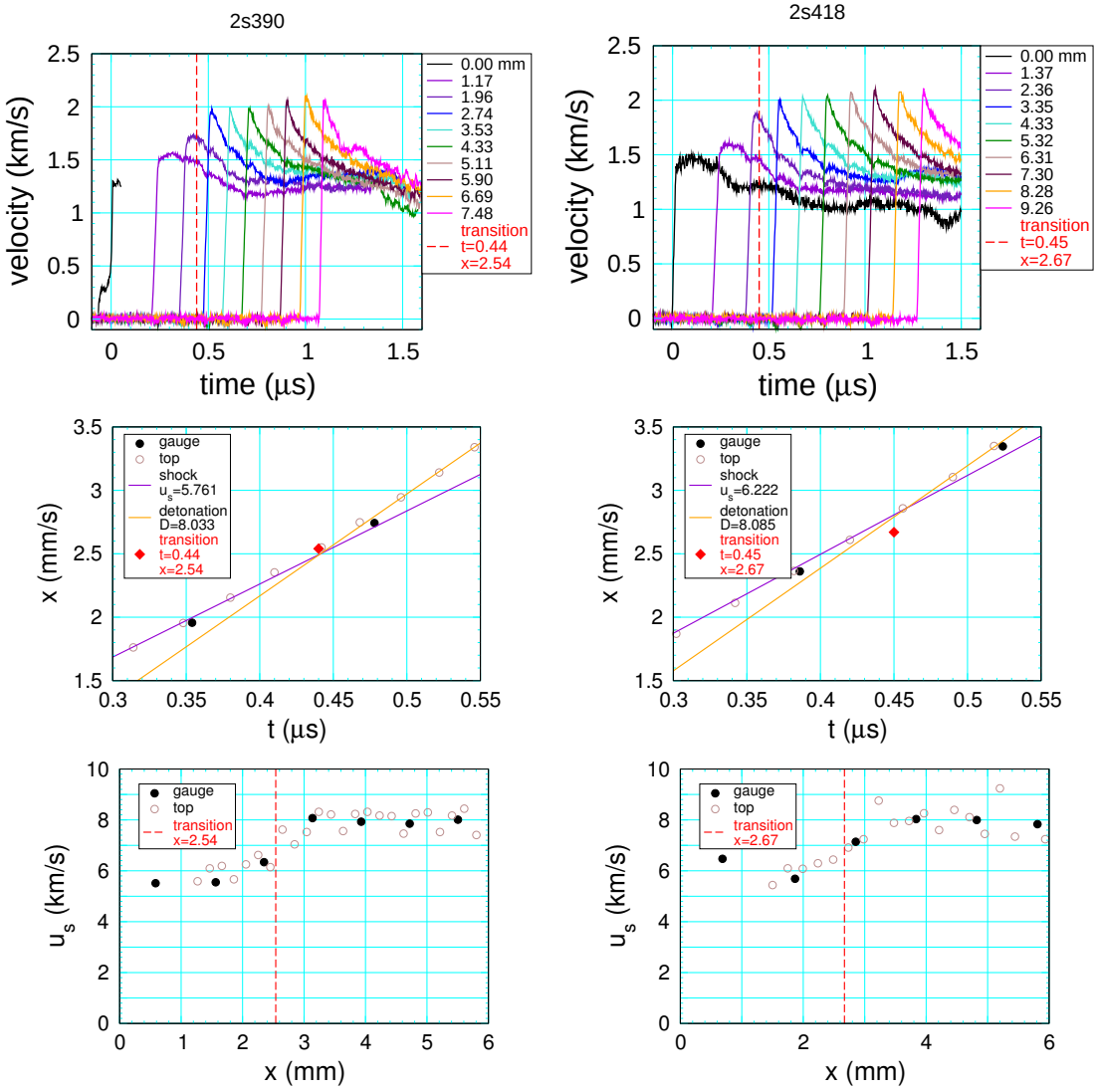

Figure 12: Gauge data for outlier shots 2s390 and 2s418. Top plot is velocity gauge data. Vertical dashed red line is transition time from [Gustavsen et al., 2017, table I]. Middle plots are tracker data and shock jump off time from the velocity gauges. The orange and magenta lines correspond to fits of the first 10 data point and 10 data points after transition to detonation, respectively. Transition point from [Gustavsen et al., 2017, table I] is denoted by red diamond. Bottom plots are finite difference shock velocity from the tracker gauges.

in the transition may be due to tilt. We also note that the detonation speed after transition (8.04 km/s) is higher than for the cold shot shown in fig. 10. Due to thermal expansion, higher temperatures have a the lower density, and hence the CJ detonation speed is lower. The higher hot detonation speed may be a transient response due to higher burn rate.

3.4 Other data

For the remaining 2 cases (very cold and very hot) shown in fig. 1, there is only 1 lot for each case and no outliers. The rms relative errors listed in table 1 are slightly lower than the other cases. There are also fewer data points (5 and 3), which are not enough to have good statistics for the uncertainty.

4 Temperature interpolation

The Pop plot parameters in table 1 can be smoothly interpolated as function of temperature using an Akima spline [Akima, 1970] as shown in fig. 13. The resulting Pop plots at selected temperatures are shown in fig. 14. We note that up to the PBX 9502 CJ pressure of 28 GPa the lines for different temperatures do not cross. The interpolated Pop plots can be used to calibrate burn rates for pressures in the shock initiation regime.

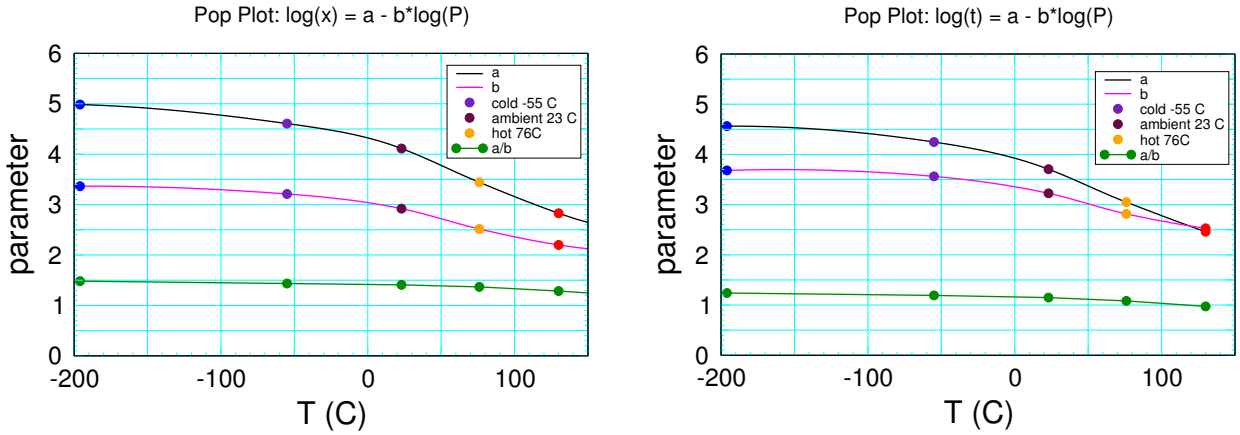

Figure 13: Temperature interpolation of Pop plot parameters for PBX 9502.

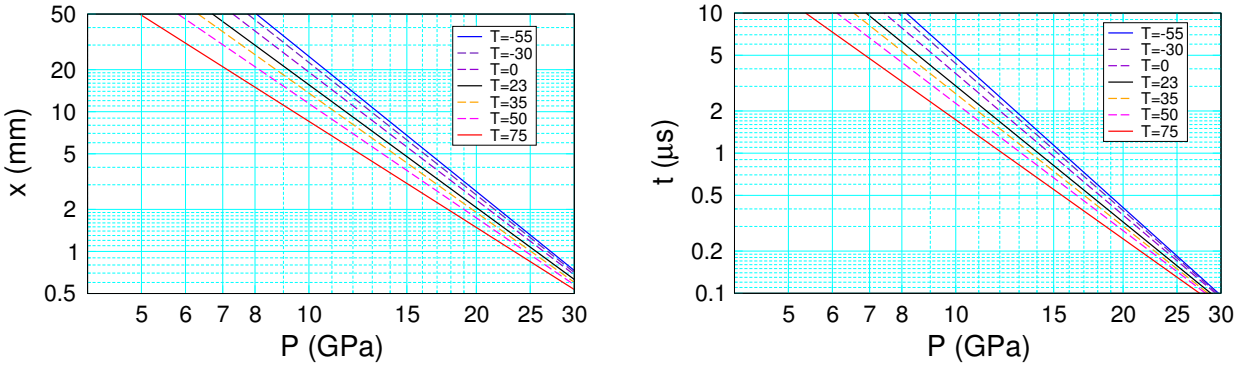

Figure 14: Interpolated Pop plots for PBX 9502 at selected temperature in range -55 to 76 C.

It is interesting to note that as a function of temperature the ratio of Pop plot parameters A/B are nearly constant. However, distance-to-run is

$$x/\text{mm} = 10^{A_x}(P/\text{GPa})^{-B_x} \ . \tag{6}$$

Consequently, the parameter A_x and hence the ratio A_x/B_x depends on the chosen units for x and P. Similarly for time to detonation A_t and A_t/B_t depend on units for t and P.

5 Summary

There are a total of 99 Pop plot data points for PBX 9502. Divided up among 5 initial temperatures and several different lots the number of data points varies from 3 to 18 with most cases being in the 4 to 7 range. Consequently, most cases do not have enough data points to get good statistics for the scatter of around the Pop plot fits.

The data is sufficient to show a systematic difference with temperature. Shock sensitivity increases and the slope of the Pop plot decreases with increasing temperature. For the cold temperature (-55 C), there are significant differences in the Pop plot with 2 out of 5 of lots.

Neglecting outliers, the scatter in the data for each lot has a root mean square relative error of less than 7 %. This is compatible with the estimated experimental uncertainty in determining the initial shock pressure and resulting from small misalignments of the drive system with the HE sample. The fits to both run distance and time to detonation have a comparable scatter. This implies the run distance as a function of the detonation time has a power-law behavior.

There are a total of 11 outliers, defined as having a relative error greater than twice the root mean square error of the fit. The outliers have a root mean square error of 20 to 30 %. For

the gas gun experiments the gauge data is available on the small scale database. For the wedge experiment detailed data is available for only 1 of the outliers. An examination of the outlier indicates that at least half of the relative error is due to the subjective choice of the transition point.

For ambient temperature, the Pop plot fit to wedge experiment data is within the variation of the fits to the gas gun experiment data for different lots. For the cold temperature the variation of the Pop plot with lot is likely due to differences in grain scale heterogeneities that effect the burn rate. This would imply that an accurate burn model for shock initiation would need to be calibrated for the specific lot to be used in an application.

The Pop plot fits at the measured temperatures can be interpolated to obtain Pop plot fit parameters in the standard operating range of -55 C to 75 C. This can be used to estimate uncertainty in the measurements with small variations in the initial temperature, and for reactive burn models to calibrate the temperature dependence of shock initiation.

Finally we note that while the Pop plot is arguable the most important characterization of shock initiation, it only applies to initiation in 1-D driven by a sustained shock. Initiation for other more complicated drive conditions can be important for applications. These include multiple shocks which are related to shock desensitization, a shock of limited duration or short shock generated by a thin flyer plate, a shock followed by a rarefaction as occurs in the gap test [see for example, Gibbs and Popolato, 1980, part II, §4.2], and initiation of a booster by a detonator for which divergence of the lead shock is important.

References

H. Akima. A new method of interpolation and smooth curve fitting based on local procedures. *Journal of the ACM*, 17:589–602, 1970. URL https://doi.org/10.1145/321607.321609. 20

C. L. Armstrong and J. T. Mang. In-situ small- and utra-small angle neutron scattering of heated PBX 9502. In *Sixteenth Symposium (International) on Detonation*, 2018. URL http://permalink.lanl.gov/object/tr?what=info:lanl-repo/lareport/LA-UR-18-26152. 9

A. W. Campbell. Diameter effect and failure diameter of a TATB-based explosive. *Propellants, Explosives, Pyrotechnics*, 9:183–187, 1984. URL https://doi.org/10.1002/prep.19840090602. 11

A. W. Campbell, W. C. Davis, J. B. Ramsay, and J. R. Travis. Shock initiation of solid explosives. *Phys. Fluids*, 4:511–521, 1961. URL https://doi.org/10.1063/1.1706354. 2

J. C. Dallman and J. Wackerle. Temperature-dependent shock initiation of TATB-based high explosive. In *Tenth Symposium (International) on Detonation*, pages 130–138, 1993. 3, 7

J. J. Dick, C. A. Forest, J. B. Ramsay, and W. L. Seitz. The Hugoniot and shock sensitivity of a plastic-bonded TATB explosive PBX 9502. *J. Appl. Phys*, 63:4881–4888, 1988. URL https://doi.org/10.1063/1.340428. 2, 14

J. J. Dick, A. R. Martinez, and R. S. Hison. Plane impact response of PBX 9501 and its components below 2 GPa. Technical report, Los Alamos National Lab., April 1998. LA-13426-MS, https://doi.org/10.2172/663187. 4

J. J. Dick, D. E. Hooks, R. Menikoff, and A. R. Martinez. Elastic-plastic wave profiles in cyclotetramethylene tetranitramine crystals. *J. Appl. Phys*, 96:374–379, 2004. URL https://doi.org/10.1063/1.1757026. 4

T. R. Gibbs and A. Popolato, editors. *LASL Explosive Property Data*. Univ. of Calif. Press, 1980. URL http://lib-www.lanl.gov/ladcdmp/epro.pdf. 2, 3, 7, 22

R. L. Gustavsen, S. A. Sheffield, R. R. Alcon, J. W. Forbes, C. M. Tarver, and F. Garcia. Embedded electromagnetic gauge measurements and modeling of shock initiation in the TATB based explosives LX-17 and PBX 9502. In *AIP Conference Proceedings 620, 1019*, 2002. URL https://doi.org/10.1063/1.1483711. 5

R. L. Gustavsen, R. J. Gehr, W. L. Seitz, S. A. Sheffield, R. R. Alcon, D. L. Robbins, and B. A. Barker. Shock initiation of the TATB-based explosive PBX 9502 cooled to -55 C. In *Thirteenth (International) Symposium on Detonation*, pages 970–979, 2005. 2, 17

R. L. Gustavsen, S. A. Sheffield, and R. R. Alcon. Measurements of shock initiation in the tri-amino-tri-nitro-benzene based explosive PBX 9502: Wave forms from embedded gauges and comparison of four different material lots. *J. Appl. Phys.*, 99:114907, 2006. URL https://doi.org/10.1063/1.2195191. 2, 3, 5, 11, 12, 13

R. L. Gustavsen, D. G. Thompson, B. W. Olinger, R. DeLuca, B. D. Bartram, T. H. Pierce, and N. J. Sanchez. Shock initiation experiments on ractchet grown PBX 9502. In *Fourteenth Symposium (International) on Detonation*, pages 655–663, 2010. 9

R. L. Gustavsen, R. J. Gehr, S. M. Bucholtz, R. R. Alcon, and B. D. Bartram. Shock initiation of triaminotrinitrobenzene base explosive PBX 9502 cooled to -55 C. *J. Appl. Phys.*, 112, 2012. URL https://doi.org/10.1063/1.4757599. 2, 5, 16, 17

R. L. Gustavsen, R. J. Gehr, S. M. Bucholtz, A. H. Pacheco, and B. D. Bartram. Shock initiation of the TATB-based explosive PBX 9502 heated to 76 C. In *AIP Conference Proceedings 1793, 030017*, 2017. URL https://doi.org/10.1063/1.4971475. 3, 19

R. L. Gustavsen, B. D. Bartram, L. L. Gibson, A. H. Pacheco, J. D. Jones, and A. B. Goodbody. Shock initiation of the TATB-based explosive PBX 9502 heated to 130 C. In *AIP Conference Proceedings 1979, 100015*, 2018. URL https://doi.org/10.1063/1.5044887. 3

B. C. Hollowell, R. L. Gustavsen, and D. M. Dattelbaum. Shock initiation of TATB-based explosive PBX 9502 cooled to 77 Kelvin. *J. Phys. Conf. Series*, 500, 2014. URL https://doi.org/10.1088/1742-6596/500/18/182014. 2

E. L. Lee and C. M. Tarver. Phenomenological model of shock initiation in heterogeneous explosives. *Phys. Fluids*, 23:2362–272, 1980. URL https://doi.org/10.1063/1.862940. 2

J. L. Maienschein and F. Garcia. Thermal expansion of TATB-based explosives from 300 to 566 K. *Thermochimica Acta*, 384:71–83, 2002. URL https://doi.org/10.1016/S0040-6031(01)00778-X. 3

R. Menikoff and M. S. Shaw. Reactive burn models and Ignition & Growth concept. *EPJ Web of Conferences*, 10, 2010. URL https://doi.org/10.1051/epjconf/20101000003. 2

J. B. Ramsay and A. Popolato. Analysis of shock wave and initiation data for solid explosives. In *Fourth Symposium (International) on Detonation*, pages 233–238, 1965. 2

K. S. Vandersall, C. M. Tarver, F. Garcia, and S. K. Chidester. On the low pressure shock initiation of octahydro-1,3,5,7-tetranito-1,3,5,7-tetrazocine based plastic bonded explosives. *J. Appl. Phys.*, 107:094906, 2010. URL https://doi.org/10.1063/1.3407570. 4